# First Record of Oceanic Anoxic Event 1d at Southern High Latitudes: Sedimentary and Geochemical Evidence From International Ocean Discovery Program Expedition 369

Qingchao Fan, Zhaokai Xu, Kenneth G. Macleod, Hans-Jürgen Brumsack, Tiegang Li, Fengming Chang, Shiming Wan, Laurent Riquier, Delong Fu, Zhendong Luan, et al.

Geophysical Research Letters

RESEARCH LETTER
10.1029/2021GL097641

# First Record of Oceanic Anoxic Event 1d at Southern High Latitudes: Sedimentary and Geochemical Evidence From International Ocean Discovery Program Expedition 369

**Qingchao Fan[1,2,3,4,5], Zhaokai Xu[1,2,3,4], Kenneth G. MacLeod[6], Hans-Jürgen Brumsack[7], Tiegang Li[2,8], Fengming Chang[1,2,4], Shiming Wan[1,2,3], Laurent Riquier[9], Delong Fu[10], Zhendong Luan[1,4], Baichuan Duan[2,8], Hongjin Chen[1,5], Wei Wang[1,5], and Dhongil Lim[11]**

[1]Key Laboratory of Marine Geology and Environment, Institute of Oceanology, Chinese Academy of Sciences, Qingdao, China, [2]Laboratory for Marine Geology, Pilot National Laboratory for Marine Science and Technology (Qingdao), Qingdao, China, [3]CAS Center for Excellence in Quaternary Science and Global Change, Xi'an, China, [4]Center for Ocean Mega-Science, Chinese Academy of Sciences, Qingdao, China, [5]University of Chinese Academy of Sciences, Beijing, China, [6]Department of Geological Sciences, University of Missouri, Columbia, MO, USA, [7]Institut für Chemie und Biologie des Meeres (ICBM), Carl von Ossietzky Universität Oldenburg, Oldenburg, Germany, [8]Key Laboratory of Marine Sedimentology and Metallogeny, First Institute of Oceanography, Ministry of Natural Resources, Qingdao, China, [9]Institut des Sciences de la Terre de Paris (ISTEP), Sorbonne Université, Paris, France, [10]College of Meteorology and Oceanography, National University of Defense Technology, Changsha, China, [11]South Sea Research Institute, Korea Institute of Ocean Science & Technology, Geoje, Republic of Korea

**Abstract** Oceanic anoxic event 1d (OAE 1d) has been well studied at northern low latitudes (i.e., in Tethys and the North Atlantic); however, the paleoenvironmental response to this event at high latitudes has not been documented and the triggering mechanism remains unknown. Here, we address both of these shortcomings by presenting the first detailed sedimentary and multi-proxy geochemical record of the OAE 1d at southern high latitudes (60–62°S), obtained from sediments using Site U1513, IODP Expedition 369. Biostratigraphic and chemostratigraphic data support correlation of the interval studied with OAE 1d, and the sedimentary mercury proxy reveals that at least at Site U1513, OAE 1d is associated with the Central Kerguelen large igneous province volcanism. Furthermore, the significant increase in continental runoff and consequent terrigenous input from southwestern Australia in the southeastern proto-India Ocean might have resulted in regionally weakened bottom-water oxygenation and strengthened organic matter burial during OAE 1d.

**Plain Language Summary** Geological marine records hold valuable information that could inform predictions for the future of our warming world. Marine sediments are an important reservoir of the global organic carbon and changes at the seafloor can modulate release of $CO_2$ into the atmosphere. Cretaceous oceanic anoxic event 1d (~latest Albian) was a significant disturbance to the global carbon cycle in the mid-Cretaceous although it is poorly documented in the southern hemisphere especially at high latitudes. Our integrative sedimentary-geochemical study demonstrates that oceanic anoxic event 1d at southern high latitudes might have been directly triggered by Central Kerguelen large igneous province volcanism. Volcanic emissions are proposed to have shifted the climate such that runoff and input of terrigenous sediment from southwestern Australia increased. These changes would have weakened bottom-water oxygenation and increased organic matter burial in the southeastern proto-Indian Ocean.

Qingchao Fan, Zhaokai Xu, Kenneth G. MacLeod, Hans-Jürgen Brumsack, Tiegang Li, Fengming Chang, Shiming Wan, Laurent Riquier, Delong Fu, Zhengdong Luan, Baichuan Duan, and Hongjin Chen contributed equally to this work.

**Key Points:**

- We present the first sedimentary and geochemical records for oceanic anoxic event 1d at southern high latitudes (60–62°S)
- Environmental changes during oceanic anoxic event 1d might be directly triggered by Central Kerguelen large igneous province volcanism
- Multiple paleoenvironmental changes occurred in the study area during oceanic anoxic event 1d

**Supporting Information:**

Supporting Information may be found in the online version of this article.

**Correspondence to:**

Z. Xu and D.lim,
zhaokaixu@qdio.ac.cn;
oceanlim@kiost.ac.kr

**Citation:**

Fan, Q., Xu, Z., MacLeod, K. G., Brumsack, H.-J., Li, T., Chang, F., et al. (2022). First record of oceanic anoxic event 1d at Southern high latitudes: Sedimentary and geochemical evidence from International Ocean Discovery Program Expedition 369. *Geophysical Research Letters*, *49*, e2021GL097641. https://doi.org/10.1029/2021GL097641

Received 7 JAN 2022
Accepted 29 APR 2022



## 1. Introduction

The mid-Cretaceous (90–110 Ma) was a hot greenhouse period characterized by high rates of submarine volcanism including ocean crust production at mid-ocean ridges. This volcanism was accompanied by high concentrations of atmospheric $CO_2$, significant sea level rise, and an accelerated hydrological cycle (Foster et al., 2017; Haq, 2014; Jenkyns, 2010; Tierney et al., 2020). $CO_2$ concentrations reached levels approximately 700–2,000 ppmv (2.5–7 times higher than preindustrial values; Foster et al., 2017 and references therein), and, consistent with high $pCO_2$ levels, sea surface temperatures have been estimated to have reached ~30–32°C at 60°S latitude (Bice et al., 2003; Huber et al., 2018), much higher than modern-era temperatures of ~0–1°C at these latitudes (data from Ocean Data View). Contemporary latitudinal temperature gradients were reduced to <14°C, much smaller than the present difference between tropical polar latitudes of ~20°C (O'Brien et al., 2017 and references

therein). This interval also includes a series of oceanic anoxic events (OAEs), critical paleoenvironmental events characterized by regionally to globally distributed black shale deposition, significant carbon isotope excursion, and intense disruption of marine ecosystems occurred during this interval (Jenkyns, 2010; Lowery et al., 2020; Schlanger & Jenkyns, 1976).

OAEs are defined as short-lived periods of large increases in organic carbon deposition in extensive deep-sea and hemipelagic settings (Breheret, 1988; Jenkyns, 2010; Schlanger & Jenkyns, 1976). The main Cretaceous OAEs occurred during the early Aptian (OAE 1a, ~120 Ma), the early Albian (OAE 1b, ~111 Ma), the mid-Albian (OAE 1c, ~105 Ma), the latest Albian (OAE 1d, ~101 Ma), the Cenomanian-Turonian boundary (OAE 2, ~94 Ma), and the Coniancian-Santonian boundary (OAE 3, ~86 Ma; Jenkyns, 2010). To date, fewer studies have addressed minor OAEs such as OAEs 1b, 1c, 1d and 3 than main OAEs 1a and 2. This bias in the literature is likely due to emphasis on the largest events and the greater difficulty of studying the minor events than the major ones because the organic-rich shales of the former are less widely distributed than those of the latter and the associated isotopic excursions are less dramatic or harder to resolve (Li et al., 2016; Navarro-Ramirez et al., 2015; Rodríguez-Cuicas et al., 2019).

Previous studies have shown that OAE 1d is characterized by a positive carbon isotope excursion (~0.5–1.5‰) in carbonate and organic carbon, elevated contents of total organic carbon content (TOC, ~1%–2%), and increased turnover rates in planktic foraminifera and radiolaria (Erbacher & Thurow, 1997; Richey et al., 2018; Wilson & Norris, 2001; Yao et al., 2018). This event was also accompanied by an accelerated hydrological cycle, intensified continental chemical weathering and terrigenous supply, increased nutrient discharge to the ocean, and enhanced upwelling and primary productivity in the sea (Charbonnier et al., 2018; Jenkyns, 2010; Rodríguez-Cuicas et al., 2020). Regarding the forcing mechanisms of OAE 1d, the eruption of the Central Kerguelen large igneous province may have driven the onset of this anoxic event (Yao et al., 2021). In addition, the formation of organic-rich shales during OAE 1d may have resulted from stimulated primary productivity (Wilson & Norris, 2001 and references therein) and/or increased organic matter (OM) preservation in a stagnant water column with low bottom-water oxygenation (Wilson & Norris, 2001). To better understand if and how volcanism resulting in large igneous provinces could drive major events like OAE 1d, environmental consequences associated with pulse of volcanism need to be further constrained (Koppers and Coggon, 2020). Unfortunately, there is no consensus on specific events and/or processes that forced OAE 1d.

Spatially, OAE 1d has been well documented in the Tethys (Bornemann et al., 2005; Erbacher & Thurow, 1997; Pavlishina, 2017; Yao et al., 2018), in the Boreal realm (Bornemann et al., 2017) and in the Atlantic Ocean (Giorgioni et al., 2015; Rodríguez-Cuicas et al., 2020; Wilson & Norris, 2001). It has also been identified in North America (Gröcke et al., 2006; Richey et al., 2018; Scott et al., 2013) and the subequatorial Pacific (Navarro-Ramirez et al., 2015). However, a continuous sedimentary record across OAE 1d at high southern latitudes (>60°) has not been reported previously.

In this study, we present the first continuous detailed sedimentary and geochemical records for OAE 1d at southern high latitudes (60–62°S) in the Mentelle Basin off the SW coast of Australia (Figure 1a) (Huber et al., 2019). The data collected are used to (a) identify changes in the source of siliciclastic sediments and OM in the Mentelle Basin; (b) reconstruct the terrigenous input, marine primary productivity, bottom-water redox conditions, and OM burial rates in the basin; and (c) investigate the possible forcing mechanisms for OAE 1d.

## 2. Materials and Methods

The Mentelle Basin, a large (36,000 $km^2$), deep-water (500–4,000 m) basin, forms a key component of the extensional rift system on the southwestern margin of Australia that developed during Mesozoic breakup of eastern Gondwana (Figure S1a in Supporting Information S1; Borissova et al., 2010). During the mid-Cretaceous and before the onset of Australia-Antarctica breakup, the basin was located at southern high paleolatitudes (60–62°S) and surrounded by the Australia-Antarctica and Indian Plates (Borissova et al., 2010; Huber et al., 2019). Thus, this basin was well located to preserve a record of the paleoceanographic and paleoenvironmental evolution of the region.

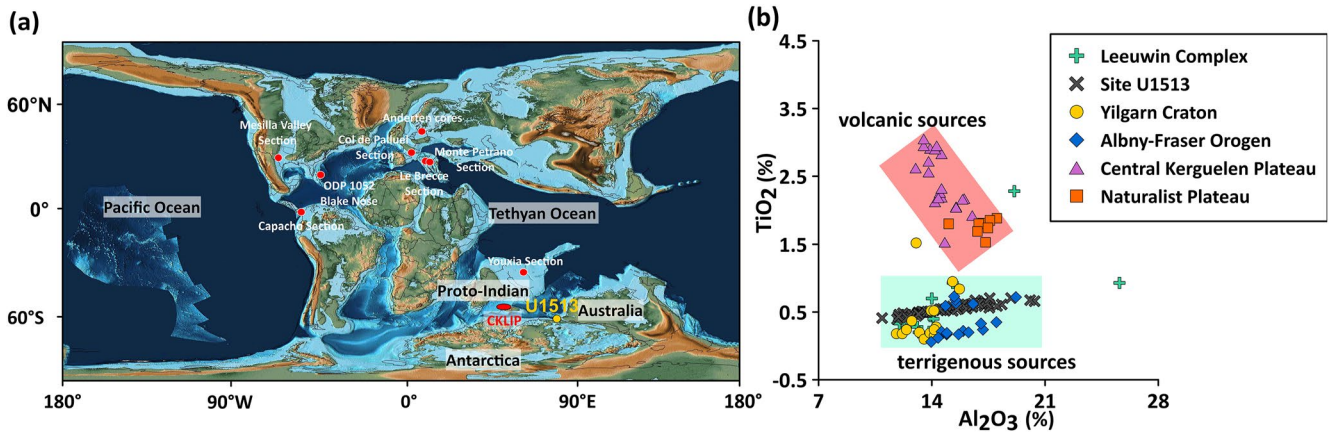


**Figure 1.** (a) Paleogeographic map at the Albian-Cenomanian boundary (~100 Ma; modified from Scotese (2016), https://www.earthbyte.org/category/resources/data-models/paleogeography/) showing the location of Site U1513. CKLIP = Central Kerguelen large igneous province. (b) Discrimination plot of $Al_2O_3$ versus $TiO_2$ for the studied sediments at Site U1513. Values of rock samples from potential sources, including the Leeuwin Complex (Wilde & Nelson, 2001), Yilgarn Craton (Chen et al., 2003; Qiu et al., 1999), Albany-Fraser Orogen (Kirkland et al., 2015), Central Kerguelen Plateau (Neal et al., 2002), and Naturaliste Plateau (Pyle et al., 1995; Storey, 1992), are also shown for comparison.

Site U1513 (latitude: 33°47.6084′S, longitude: 112°29.1338′E) was drilled with a high recovery rate (80.8%) on the northwestern margin of the Mentelle Basin by International Ocean Discovery Program (IODP) Expedition 369 in 2017 (Figure S1a in Supporting Information S1; Huber et al., 2019). Current water depth is ~2,800 m, and the core penetrates to a total of 774 m below the seafloor. This study addresses the interval from 277 to 333 m below the seafloor in Hole U1513D, and we focus on analyses of 60 typical samples selected from the interval. Overall, the sediments of the studied interval are dominated by black claystone and nannofossil-rich claystone that frequently include some shell fragments and pyrite grains (Huber et al., 2019).

The siliciclastic sediment fractions of the selected 60 bulk sediments were extracted according to the sequential leaching method reported by Xu et al. (2018). Major and trace element (including rare earth element) compositions of the resulted materials were measured using an inductively coupled plasma optical emission spectrometer (Varian 720ES) and an inductively coupled plasma mass spectrometer (Varian 820) at the Qingdao Sparta Analysis & Test Company Limited (Zhang et al., 2021), with relative deviations of <5% for major and trace elements. In addition, grain-size analysis was conducted on the siliciclastic sediment fractions of the same 60 samples using a Cilas 940L laser particle size analyzer in the Key Laboratory of Marine Geology and Environment, Institute of Oceanology, Chinese Academy of Sciences. This apparatus could measure grain sizes ranging from 0.3 to 2,000 μm with an analytical precision of <2% (Wan et al., 2017).

A subset of 35 bulk sediments were measured for the contents of total carbon (TC), total nitrogen (TN), total sulfur (TS), total Hg, biogenic silica (BSi), and calcium carbonate ($CaCO_3$) at the South Sea Research Institute, Korea Institute of Ocean Science & Technology, with the same analytical methods and accuracy as those reported by Lim et al. (2017). The contents of TC, TN, and TS were measured using a Carlo Erba Elemental Analyzer 1108, and the concentration of the total inorganic carbon (TIC) was determined using a $CO_2$ Coulometer (CM5014), with a relative analytical error of <5%. The $CaCO_3$ and $Ca_{biologic}$ contents were calculated from the TIC concentration by using a multiplication factor of 8.333 and 3.333, respectively (Lim et al., 2017; Xu et al., 2018). The TOC content was calculated as the difference between the TC and TIC concentrations. The Hg concentration was measured using a Hydra II C direct Hg analyzer, with analytical accuracy and precision of <5% and <10%, respectively. The BSi content was analyzed using a wet alkaline extraction method modified from Mortlock and Froelich (1989) and Müller and Schneider (1993), and the relative analytical error was <10%.

In addition, the $SiO_2$ contents of 53 bulk samples and the concentrations of U in six bulk samples were analyzed using a wavelength-dispersive X-ray fluorescence (Panalytical PW 2400) and an inductively coupled plasma mass spectrometer (Finnigan MAT Element II), respectively, at the Institute for Chemistry and Biology of the Marine Environment, University of Oldenburg. Analytical precision is better than 5% for $SiO_2$ and 7.6% for U

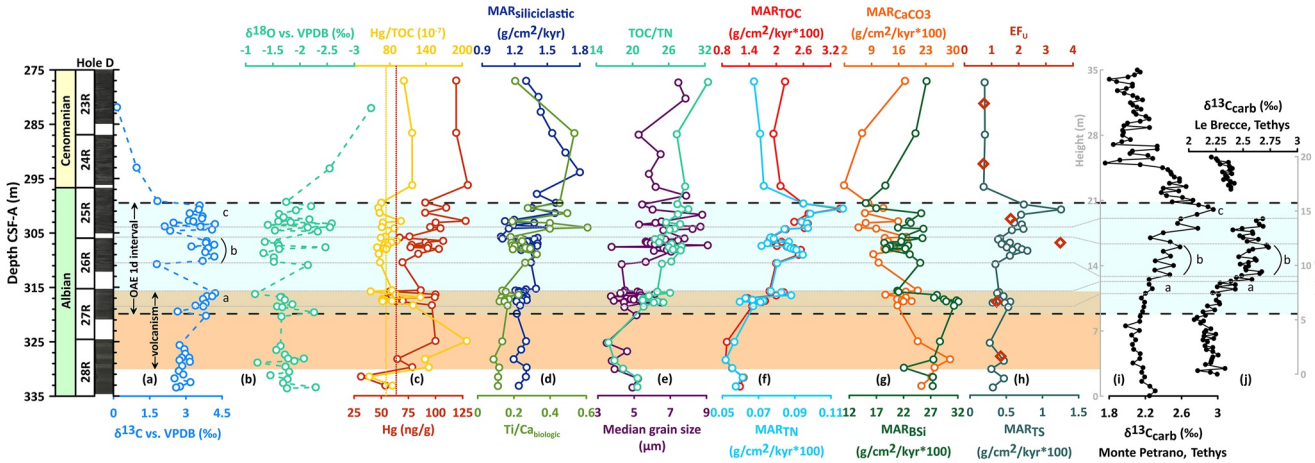


**Figure 2.** Comparisons among (a) carbonate $\delta^{13}C$; (b) carbonate $\delta^{18}O$; (c) Hg/TOC ratio and Hg concentration; (d) $MAR_{siliciclastic}$ and $Ti/Ca_{biologic}$ ratio; (e) TOC/TN ratio and median grain size; (f) $MAR_{TOC}$ and $MAR_{TN}$; (g) $MAR_{CaCO_3}$ and $MAR_{BSi}$; and (h) $EF_U$ and $MAR_{TS}$ at Site U1513, (i) carbonate $\delta^{13}C$ from the Monte Petrano section, Tethys (Gambacorta et al., 2015), and (j) carbonate $\delta^{13}C$ from the Le Brecce section, Tethys (Gambacorta et al., 2015). $MAR_{siliciclastic}$ = siliciclastic mass accumulation rate. $MAR_{(TOC;\,TN;\,CaCO_3;\,BSi;\,TS)}$ = mass accumulation rate of (TOC; TN; $CaCO_3$; BSi; TS). $EF_U$ = enrichment factor of U. The red dotted line and the blue dotted line are the mean values of Hg content and Hg/TOC ratio, respectively, of reported sedimentary rocks (Grasby et al., 2019).

(März et al., 2013; Turgeon & Brumsack, 2006). Accuracy was monitored by the parallel analysis of international and in-house reference materials.

The siliciclastic mass accumulation rate ($MAR_{siliciclastic}$) was calculated via the following equation: $MAR_{siliciclastic}$ = siliciclastic sediment fraction percentage (%) × dry bulk density (g/cm$^3$) × linear sedimentation rate (cm/kyr; Rea & Janecek, 1981). In addition, the mass accumulation rates of TOC ($MAR_{TOC}$), TN ($MAR_{TN}$), TS ($MAR_{TS}$), $CaCO_3$ ($MAR_{CaCO3}$), and BSi ($MAR_{BSi}$) were calculated by the same principle. The dry bulk density with a range of 1.084 g/cm$^3$ to 1.149 g/cm$^3$ and chronological data are cited from the shipboard report (Huber et al., 2019).

## 3. Results

The microfossil biostratigraphy for Site U1513 is built using calcareous nannofossil bioevents (Table S1 in Supporting Information S1) and demonstrates that the studied sediment section spans the upper Albian-lower Cenomanian, including the OAE 1d event (Huber et al., 2019). The carbonate $\delta^{13}C$ values exhibit a positive excursion (average: 1.6‰, range: 2.65–4.21‰) in the sediment interval of 300–320 m in the core (Edgar et al., 2022). In addition, this sediment interval, corresponding to OAE 1d, is characterized by a negative $\delta^{18}O$ excursion of ~0.9‰ (Figure 2) and a remarkably high TOC contents (maximum ~1.8% in the depth interval of ~300–320 m) relative to intervals above and below the $\delta^{13}C$ excursion (Edgar et al., 2022).

$MAR_{siliciclastic}$, $Ti/Ca_{biologic}$ ratio, and median grain size display significant increasing trends from ~300 to 320 m (Figure 2). Significant sedimentary organic proxies—$MAR_{TOC}$, $MAR_{TN}$, $MAR_{TS}$, and TOC/TN ratio—show high values and similar trends of higher values over the ~300–320 m interval (Figure 2). $MAR_{CaCO3}$ and $MAR_{BSi}$ display high values between ~317 and 331 m and decreasing values from ~300 to 320 m (Figure 2). In addition, the redox proxy of authigenic U, defined as $(U/Al)_{sample}/(U/Al)_{upper\ continental\ crust\ (UCC);}$ Taylor & Mclennan, 1985), is in agreement with $MAR_{TS}$ characterized by a higher time resolution (Figure 2) and Hg concentrations largely increase in these sediments (Figure 2).

## 4. Discussion

### 4.1. Recognition of OAE 1d

The OAE 1d interval in Hole U1513D is proposed to span from the initial excursion in carbonate $\delta^{13}C$ values at ~320 m CSF-A to ~300 m CSF-A where carbonate $\delta^{13}C$ values start a definitive downward trend (Figure 2). The carbonate $\delta^{13}C$ excursion and elevated TOC levels observed at Site U1513 are comparable to typical OAE

1d records from the Atlantic/Tethyan basins and surrounding continents (Bornemann et al., 2005, 2017; Gale et al., 2011; Wilson & Norris, 2001; Yao et al., 2021), with the records from the Tethyan Monte Petrano and Le Brecce sections (Gambacorta et al., 2015, 2020) shown for reference (Figure 2). Further, biostratigraphic control including the presence in Hole U1513D, core 26 of *Thalmanninella appenninica*, a foraminiferal species used for identifying OAE 1d (Table S1 in Supporting Information S1, Huber et al., 2019), demonstrates chronostratigraphic correlation between the record at Site U1513 and OAE 1d documented elsewhere.

Documenting OAE 1d in these samples makes Site U1513 the first detailed, seemingly complete sediment sequence of OAE 1d to be identified in the austral realm. Thus, an important contribution of this study is confirmation that OAE 1d was a global event (Jenkyns, 2010; Yao et al., 2021).

Placing the upper limit of the OAE 1d $\delta^{13}C$ excursion is complicated by an interval of quite low $\delta^{13}C$ values above the 295 m CSF-A (Edgar et al., 2022) that correlates with quite low carbonate content and an absence of foraminifera. In low carbonate intervals, bulk carbonate isotopic values are susceptible to diagenetic overprints with low $\delta^{13}C$ values due to the incorporation of remineralized organic carbon. The transition into the proposed OAE 1d interval, though, does not correspond to a change in carbonate content, diagenetic alteration would be unlikely to result in a positive excursion, and foraminifera present under microscope shows no change in preservation between the interval below and within the proposed OAE 1d $\delta^{13}C$. However, until ongoing foraminiferal isotopic and scanning electronic microscope studies are complete, consider the bulk carbonate $\delta^{13}C$ only has a chemostratigraphic indicator confirmed by biostratigraphy. We use elemental data to provide evidence of the paleoceanographic and paleoenvironmental expression of OAE 1d at southern high latitudes.

### 4.2. Siliciclastic Sediment Provenance

The final stages of breakup between Greater India and Australia-Antarctica occurred during the Hauterivian through early Aptian, and the southwest Australia rifted margin including the Mentelle Basin experienced syn-rift subsidence interval and two-phase postrift subsidence process (Lee et al., 2020). Sedimentation in the Mentelle Basin during the early Albian through middle Cenomanian was characterized by deposition of black claystones and nannofossil-rich claystones (Huber et al., 2019). That is, fine grained terrigenous material dominates sediment input. However, sediment provenance within the Mentelle Basin deposits covering the mid-Cretaceous has not been clearly defined.

Previous mineralogical, geochemical, and geochronological studies on sediments retrieved from the nearby Perth Basin revealed that the regionally extensive Yilgarn Craton, Leeuwin Complex, and Albany-Fraser Orogen are the main sources for a sequence of rift basins along the southwestern margin of Australia (Cawood & Nemchin, 2000; Descourvieres et al., 2011; Dillinger et al., 2018; Olierook et al., 2019). The Yilgarn Craton is mainly composed of Archaean granites, together with volcanic greenstone belts, in the central part of Western Australia (Cassidy et al., 2006). The Leeuwin Complex, separated from the Perth Basin by the Dunsborough Fault to the east, consists predominantly of Proterozoic felsic gneisses (Wilde & Nelson, 2001). Moreover, the Albany-Fraser Orogen, a component of the West Australia Craton, is predominated by Mesoproterozoic orthogneisses and granitic rocks (Smithies et al., 2015). Considering the synchronous formation of both the Central Kerguelen Plateau (~Albian-Cenomanian Boundary) and our studied sediment sequence, together with the potentially large radius of influence for the mantle plume (~500–1,000 km) related to the former, this plateau may also have been one of the sources for the studied samples (Coffin et al., 2002; Lee et al., 2020). The Naturaliste Plateau, which is thought to represent a rifted fragment of the Kerguelen large igneous province, may also have been a contributor to the Mentelle Basin detritus between the late Albian and early Cenomanian (Lee et al., 2020).

Discrimination plots of $Al_2O_3$ versus $TiO_2$ and rare earth elements are widely and effectively used to identify marine sediment provenance, especially in the context of terrigenous detritus input (Munksgaard et al., 2003; Wehausen et al., 2003). In addition to parent rock sources, various factors, such as chemical weathering on land, dilution by biogenic, organic, and authigenic components, and hydraulic sorting, can influence the major and rare earth element compositions of marine sediments (Clift, 2016). In this study, biogenic, organic, and authigenic components were effectively removed from the siliciclastic sediment fractions by sequential leaching procedures (Xu et al., 2018). Moreover, the lack of correlation between $(La/Sm)_{UCC}$ ratio ($R = 0.13$, $n = 60$, $\alpha = 0.05$) or $(Gd/Yb)_{UCC}$ ratio ($R = 0.06$, $n = 60$, $\alpha = 0.05$) and the chemical index of alteration (CIA, where

CIA=$Al_2O_3/(Al_2O_3 + CaO^* + Na_2O + K_2O) \times 100$, and CaO* represents the CaO concentration with siliciclastic origination (Nesbitt & Young, 1982)), and the lack of correlation between $(La/Sm)_{UCC}$ ratio ($R = 0.32$, $n = 60$, $\alpha = 0.05$) or $(Gd/Yb)_{UCC}$ ratio ($R = -0.49$, $n = 60$, $\alpha = 0.05$) and median grain size in the studied sediment samples (Figure S2 in Supporting Information S1) also indicate the minor influences of chemical weathering and hydraulic sorting on the elemental composition. Sediment provenance may be the most essential factor controlling the sediment compositions of major and rare earth elements.

Southwestern Australia was the primary source region of siliciclastic sediments in the Mentelle Basin during the studied interval, as indicated by the overlap in elemental composition between most sediments from Site U1513 and rock samples of the Yilgarn Craton, Leeuwin Complex, and Albany-Fraser Orogen (Figure 1b). In contrast, the much higher $TiO_2$ concentrations in source rocks from the Central Kerguelen Plateau and Naturaliste Plateau than in the studied sediment samples preclude a significant sediment contribution from either of these two plateaus during this period. These conclusions are supported by the discrimination plot of $(La/Sm)_{UCC}$ ratio versus $(Gd/Yb)_{UCC}$ ratio (Figure S1b in Supporting Information S1), revealing clear decoupling of the studied samples from sources on the Central Kerguelen Plateau and Naturaliste Plateau in rare earth element compositions. Accordingly, elemental proxies reveal that southwestern Australia (i.e., the Yilgarn Craton, Leeuwin Complex, and Albany-Fraser Orogen) was the predominant sediment contributor to Mentelle Basin detritus during the late Albian-early Cenomanian interval and the contribution from volcanic materials on the Central Kerguelen Plateau and Naturaliste Plateau seems to be limited. This single sediment source during the OAE 1d deposition in the study area simplifies inferring the paleoenvironmental influences on the sediments and their geochemical composition.

### 4.3. Volcanism Before and During the Earliest Stage of OAE 1d

Hg enrichments in sedimentary successions are a reliable indicator of volcanic activity and have been successfully used to trace the association of volcanism with OAE 1d and other OAEs (Grasby et al., 2019; Scaife et al., 2017; Yao et al., 2021). The poor correlations between the TS contents ($R = 0.12$, $n = 35$, $\alpha = 0.05$), CIA ($R = -0.18$, $n = 35$, $\alpha = 0.05$), and $MAR_{siliciclastic}$ ($R = 0.18$, $n = 35$, $\alpha = 0.05$) with the Hg contents exclude changes in the redox state, in weathering intensity, or of terrigenous detritus inputs as the dominant reasons for the high Hg enrichments (Figure S2 in Supporting Information S1; Scaife et al., 2017; Yao et al., 2021).

As shown in Figure 2, Hg contents show a ~2.5-fold increase (31–78 ng/g) from ~332 to ~331 m, followed by a gradual increasing trend upward across the studied interval. These values generally exceed the average Hg contents of sedimentary rocks (~62 ng/g; Grasby et al., 2019). Interestingly, Hg/TOC ratios remain a pronounced anomaly across an interval starting before and extending into during the earliest stage of OAE 1d (~317–331 m); but most OAE 1d sediments have Hg/TOC ratios similar to the background value ($\sim 71.9 \times 10^{-7}$, Grasby et al., 2019) of sedimentary rocks (>0.2% in TOC contents). Similar variations in volcanism-derived Hg concentrations, Hg/TOC ratios, and mass-independent Hg isotope ($\Delta^{199}Hg$) signals before and during the earliest stage of OAE 1d are found in the Youxia section, Southern Tibet (Yao et al., 2021). These results suggest that highly elevated Hg contents in the studied sediment samples at southern high latitudes prior to the onset of OAE 1d and during the earliest stage of OAE 1d are associated with enhanced volcanic activity.

Many studies proposed that elevated volcanic activity led to increasing atmospheric $CO_2$ concentrations at the onset of OAE 1d and resulted in global warming during OAE 1d (Bottini & Erba, 2018; Richey et al., 2018). For example, a substantial increase (~357 ± 150 ppmv) of atmospheric $CO_2$ concentration prior to the onset of OAE 1d has been inferred at Rose Creek Pit, USA, using multi-proxy $pCO_2$ reconstruction methods (Richey et al., 2018), for an interval that correlates with apparent increases in sea surface and thermocline temperatures in the western tropical Atlantic Ocean at this period (Petrizzo et al., 2008). Bulk carbonate $\delta^{18}O$ values do shift to lower values during OAE 1d (Figure 2), but caveats regarding interpretation of bulk carbonate isotopic $\delta^{13}C$ values discussed above also apply to $\delta^{18}O$ values. Regardless, higher atmospheric $CO_2$ concentrations suggested to begin prior to the onset of OAE 1d (Richey et al., 2018; Yao et al., 2021) combined with the significant increases of Hg contents and Hg/TOC ratios in this study (Figure 2), suggest that the trigger of OAE 1d at southern high latitudes may have been large igneous province volcanism.

### 4.4. Enhancement of Continental Runoff and Terrigenous Supply During OAE 1d

$MAR_{siliciclastic}$ and $Ti/Ca_{biologic}$ ratios have been successfully used as indicators for continental runoff and terrigenous supply to the ocean (Stuut et al., 2014; Xu et al., 2020). The stable provenance for the studied sediments precludes a potential influence of provenance on correctly deciphering continental runoff and terrigenous input proxies. This inference is also supported by the weak correlations of $MAR_{siliciclastic}$ ($R = -0.19$, $n = 60$, $\alpha = 0.05$) and $Ti/Ca_{biologic}$ ratio ($R = -0.43$, $n = 35$, $\alpha = 0.05$) with the sediment provenance proxy (i.e., $(La/Yb)_{UCC}$ ratio; Figure S2 in Supporting Information S1). Therefore, it is reasonable to conclude that the temporal variations in $MAR_{siliciclastic}$ and $Ti/Ca_{biologic}$ ratio reflect changes in continental runoff and terrigenous supply in southwestern Australia between the late Albian and early Cenomanian (Figure 2).

During OAE 1d and other Cretaceous OAEs, greenhouse climate initiated by volcanic eruptions might have accelerated the hydrological cycle on land and resulted in higher terrigenous supply to the ocean (Jenkyns, 2010; Richey et al., 2018; Rodríguez-Cuicas et al., 2020). This model explains well the stratigraphic trends in terrigenous detritus input proxies (i.e., $MAR_{siliciclastic}$, $Ti/Ca_{biologic}$ ratio, and median grain size) at Site U1513 during OAE 1d (Figure 2), indicating a considerable enhancement in continental runoff and terrigenous supply from a southwestern Australia provenance. A warm and humid climate with an enhanced hydrological cycle during OAE 1d would result in high runoff from southwestern Australia accompanied by the input of large amounts detritus and OM into the Mentelle Basin (Figure 2). Similar paleoenvironmental changes during OAE 1d are reported at northern low- (e.g., the Capacho Formation, southwestern Venezuela) and mid-latitudes (e.g., the Mesilla Valley Formation, New Mexico, USA; Jenkyns, 2010; Rodríguez-Cuicas et al., 2019; Scott et al., 2013).

### 4.5. Marine Productivity, Redox Conditions, and OM Burial During OAE 1d

Enhanced runoff from southwestern Australia and the associated increase in terrigenous material discharged into the Mentelle Basin might have resulted in significant changes in marine primary productivity, bottom-water redox conditions, and OM burial in marine sediments. Here, the records of various geochemical proxies (i.e., $MAR_{BSi}$, $MAR_{CaCO_3}$, $MAR_{TOC}$, $MAR_{TN}$, $MAR_{TS}$, $EF_U$, and TOC/TN ratio) at Site U1513 of Mentelle Basin are clearly indicative of these changes during OAE 1d. Sedimentary OM in the oceanic domain originates from marine (autochthonous) and/or terrigenous (allochthonous) sources, corresponding to distinctive TOC/TN ratios of ~6 and >10, respectively (Lim et al., 2017; Xu et al., 2020). The very high TOC/TN ratios (>20) during OAE 1d, with an increasing trend through the interval (Figure 2), indicate that OM in the studied sediments is of terrigenous origin. As shown in Figure 2, significant increases in $MAR_{TOC}$ and $MAR_{TN}$, together with the strong correlation ($R = 0.97$, $n = 27$, $\alpha = 0.05$) between them, indicate a large increase in terrestrial OM burial flux at southern high latitudes during OAE 1d.

As would be expected, other indicators for input of terrigenous detritus including $MAR_{siliclclastic}$, $Ti/Ca_{biologic}$ ratio, and median grain size also increase during OAE 1d (Figure 2). In particular, the good correlations between $Ti/Ca_{biologic}$ and $MAR_{TOC}$ ($R = 0.64$, $n = 35$, $\alpha = 0.05$) over the whole studied sediment interval indicate correlated increases in the supply of terrigenous detritus and OM (Figure S2 in Supporting Information S1). This phenomenon is most pronounced in the OAE 1d interval which is characterized by close correlations of $Ti/Ca_{biologic}$ ratio ($R = 0.65$, $n = 27$, $\alpha = 0.05$), and TOC/TN ratio ($R = 0.85$, $n = 27$, $\alpha = 0.05$) with $MAR_{TOC}$ (Figure S2 in Supporting Information S1). Consequently, the burial flux of OM in the study area during OAE 1d may be controlled mostly by terrigenous detritus and OM inputs.

The good correlation between $MAR_{BSi}$ values and bulk $SiO_{2xs}$ [$SiO_{2xs} = SiO_{2sample} - Al_{sample} \times (SiO_2/Al)_{post\text{-}Archean\ Australian\ shale}$] contents which are less affected by diagenesis argues against a diagenetic control on $MAR_{BSi}$ values in this study (Figure S3 in Supporting Information S1; März et al., 2013; Taylor & Mclennan, 1985). Interestingly, unlike terrigenous-associated proxies which increase through OAE 1d, marine productivity inferred from $MAR_{BSi}$ and $MAR_{CaCO_3}$ proxy tends to remain relatively high before and during the earliest stage of OAE 1d, but decrease during OAE 1d (Figure 2). This suggests a decrease in marine productivity during OAE 1d. High riverine input would increase the water column stratification. This change might reduce mixing of nutrient-rich deep waters from below to the surface decreasing marine primary productivity but restricting ventilation of deeper waters leading to better preservation of OM (Figure 2; Bornemann et al., 2005; van Helmond et al., 2015).

Moreover, high contents of siliciclastic fractions (60%–90%) and OM of terrigenous origin, and low contents of BSi (7%–17%), and $CaCO_3$ (1%–15%) in the sediments suggest that the Mentelle Basin was be strongly affected by terrigenous materials (detritus particles and OM) and freshwater (Xu et al., 2020). Furthermore, the negative correlations of $MAR_{CaCO_3}$ ($R = -0.61$, $n = 27$, $\alpha = 0.05$) and $MAR_{BSi}$ ($R = -0.69$, $n = 27$, $\alpha = 0.05$) with $MAR_{TOC}$ during OAE 1d support a limited contribution of marine primary productivity to the increased OM burial in the study area (Figure S2 in Supporting Information S1).

In this study, relatively high values of $MAR_{TS}$ and $EF_U$ during OAE 1d in the study area testify to a decrease in dissolved oxygen level in the bottom water of the Mentelle Basin (Figure 2; Danzelle et al., 2018; Lim et al., 2017; Suan et al., 2018). In addition, the strong correlations of $MAR_{TOC}$ ($R = 0.84$, $n = 27$, $\alpha = 0.05$) and TOC/TN ratio ($R = 0.70$, $n = 27$, $\alpha = 0.05$) with $MAR_{TS}$ suggest that the redox condition in the bottom water was likely associated with increased supplies of terrigenous OM during this period (Figure S2 in Supporting Information S1). In this stage, gradually increasing terrestrial OM input, coupled to a potential oxidation of this OM in the water column may have rapidly consumed dissolved oxygen, resulting in a decrease in oxygen level. Accordingly, the increasing concentrations of U and TS in marine sediments, potentially associated with sulfate reduction during the sedimentary process (Danzelle et al., 2018; Morse & Berner, 1995), appear upward during OAE 1d (Figure 2). In summary, our multiple proxy records illustrate that OAE 1d observed in Mentelle Basin features weakened marine primary productivity, decreased bottom-water oxygen level, and strengthened OM burial (Figure 2).

### 4.6. Forcing Mechanisms of OAE 1d at Southern High Latitudes

Volcanism of the Central Kerguelen large igneous province, together with huge amounts of $CO_2$ emissions and subsequent global warming, may have resulted in environmental perturbations on Earth that drove the onset of OAE 1d at southern high latitudes. We propose this change was the forcing mechanisms behind the regional expression of OAE 1d due to an accelerated hydrological cycle in southwestern Australia. The change in climate led to increased freshwater runoff, increased terrigenous siliciclastic sediment input, and increased input of terrestrial OM into the Mentelle Basin. The high oxygenation demand induced by the decomposition of this terrigenous OM consumed much of the dissolved oxygen in the water column. Moreover, increased input of freshwater into the Mentelle Basin caused increased stratification of the water column which in turn change would have resulted in reduced marine primary productivity but decreased ventilation due to the stronger water column stratification exacerbated oxygen depletion at the seafloor and led to enhanced OM burial in marine sediments.

## 5. Conclusions

Here, the first detailed sedimentary and geochemical records for OAE 1d at southern high latitudes are presented from IODP Site U1513 (Mentelle Basin, southwestern Australia). We reconstructed the temporal records of various paleoenvironmental proxies, including continental runoff, input and burial flux of terrigenous detritus and OM, marine primary productivity, and bottom-water redox conditions between the late Albian and early Cenomanian.

Element compositional features revealed that siliciclastic sediments deposited during OAE 1d were mainly sourced from southwestern Australia (i.e., the Yilgarn Craton, Albany-Fraser Orogen, and Leeuwin Complex). The Hg anomaly before and during the earliest stage of OAE 1d and the coeval activity of the Central Kerguelen large igneous province, demonstrated that OAE 1d might have been forced by volcanism and the associated global environmental perturbations. During OAE 1d, large amounts of terrigenous freshwater, detritus, and OM may be transported from southwestern Australia to the Mentelle Basin, which led to the decreased oxygen concentration in the bottom water, and increased OM burial in marine sediments. However, the marine primary productivity during OAE 1d at southern high latitudes was relatively limited. In particular, the relatively good consistency of the records of OAE 1d between high (i.e., this study) and low-latitudes (e.g., the Atlantic/Tethyan basins) indicates a global distribution characteristic of this event.

## Data Availability Statement

The original data presented in the study are included in the Supporting Information. Supplementary data are archived to an open-source online data repository hosted at the Zenodo database (https://doi.org/10.5281/zenodo.6358038).

**Acknowledgments**
This research used samples and shipboard data provided by the International Ocean Discovery Program. We wish to thank the editor (Sarah Feakins), Jochen Erbacher and an anonymous reviewer for providing insightful reviews. Funding for this research was provided by the Marine S&T Fund of Shandong Province for Pilot National Laboratory for Marine Science and Technology (Qingdao; 2022QNLM050203), the Strategic Priority Research Program of the Chinese Academy of Sciences (XDB42000000 and XDB40010100), the National Natural Science Foundation of China (41876034, 41676038, and 41830539), the National Special Project for Global Change and Air-Sea Interaction (GASI-GEOGE-04), the Scientific and Technological Innovation Project financially supported by the Pilot National Laboratory for Marine Science and Technology (Qingdao; 2016ASKJ13), Taishan Scholars Project Funding, and the National Research Foundation of Korea (NRF) grant (2021R1A2C1014443) funded by the Korean government.

## References

Bice, K. L., Huber, B. T., & Norris, R. D. (2003). Extreme polar warmth during the Cretaceous greenhouse? Paradox of late Turonian $^{18}O$ record at Deep Sea Drilling Project Site 511. *Paleoceanography and Paleoclimatology*, *18*(2), 1031. https://doi.org/10.1029/2002PA000848

Borissova, I., Bradshaw, B., Nicholson, C., Payne, D., & Struckmeyer, H. (2010). New exploration opportunities on the southwest Australian margin–deep-water Frontier Mentelle Basin. *APPEA Journal*, *50*, 1–13. https://doi.org/10.1071/AJ09004

Bornemann, A., Erbacher, J., Heldt, M., Kollaske, T., Wilmsen, M., Lübke, N., et al. (2017). The Albian–Cenomanian transition and Oceanic Anoxic Event 1d–an example from the boreal realm. *Sedimentology*, *64*, 44–65. https://doi.org/10.1111/sed.12347

Bornemann, A., Pross, J., Reichelt, K., Herrle, J. O., Hemleben, C., & Mutterlose, J. (2005). Reconstruction of short-term paleoceanographic changes during the formation of the Late Albian "Niveau Breistroffer" black shales (Oceanic Anoxic Event 1d, SE France). *Journal of the Geological Society*, *162*, 623–639. https://doi.org/10.1144/0016-764903-171

Bottini, C., & Erba, E. (2018). Mid-Cretaceous paleoenvironmental changes in the western Tethys. *Climate of the Past*, *14*, 1147–1163. https://doi.org/10.5194/cp-14-1147-2018

Breheret, J. G. (1988). Episodes de sédimentation riche en matière organique dans les marnes bleues d'âge aptien et albien de la partie pélagique du bassin vocontien. *Bulletin de la Societe Geologique de France*, *8*(2), 349–356. https://doi.org/10.2113/gssgfbull.iv.2.349

Cassidy, K., Champion, D., Krapez, B., Barley, M., Brown, S., Blewett, R., et al. (2006). *A revised geological framework for the Yilgarn Craton, Western Australia*. Geological Survey of Western Australia

Cawood, P. A., & Nemchin, A. A. (2000). Provenance record of a rift basin: U/Pb ages of detrital zircons from the Perth Basin, Western Australia. *Sedimentary Geology*, *134*, 209–234. https://doi.org/10.1016/s0037-0738(00)00044-0

Charbonnier, G., Adatte, T., Spangenberg, J. E., & Follmi, K. B. (2018). The expression of early Aptian to latest Cenomanian oceanic anoxic events in the sedimentary record of the Brianconnais domain. *Global and Planetary Change*, *170*, 76–92. https://doi.org/10.1016/j.gloplacha.2018.08.009

Chen, S. F., Riganti, A., Wyche, S., Greenfield, J. E., & Nelson, D. R. (2003). Lithostratigraphy and tectonic evolution of contrasting greenstone successions in the central Yilgarn Craton, Western Australia. *Precambrian Research*, *127*, 249–266. https://doi.org/10.1016/S0301-9268(03)00190-6

Clift, P. D. (2016). *Assessing Effective Provenance Methods for Fluvial Sediment in the South China Sea* (Vol. 429, pp. 9–29). Geological SocietySpecial Publications. https://doi.org/10.1144/sp429.3

Coffin, M. F., Pringle, M., Duncan, R., Gladczenko, T., Storey, M., Müller, R., et al. (2002). Kerguelen hotspot magma output since 130 Ma. *Journal of Petrology*, *43*(7), 1121–1137. https://doi.org/10.1093/petrology/43.7.1121

Danzelle, J., Riquier, L., Baudin, F., Thomazo, C., & Puceat, E. (2018). Oscillating redox conditions in the Vocontian Basin (SE France) during Oceanic Anoxic Event 2 (OAE 2). *Chemical Geology*, *493*, 136–152. https://doi.org/10.1016/j.chemgeo.2018.05.039

Descourvieres, C., Douglas, G., Leyland, L., Hartog, N., & Prommer, H. (2011). Geochemical reconstruction of the provenance, weathering and deposition of detrital-dominated sediments in the Perth Basin: The Cretaceous Leederville Formation, south-west Australia. *Sedimentary Geology*, *236*, 62–76. https://doi.org/10.1016/j.sedgeo.2010.12.006

Dillinger, A., George, A. D., & Parra-Avila, L. A. (2018). Early Permian sediment provenance and paleogeographic reconstructions in southeastern Gondwana using detrital zircon geochronology (Northern Perth Basin, Western Australia). *Gondwana Research*, *59*, 57–75. https://doi.org/10.1016/j.gr.2018.02.020

Edgar, K. M., MacLeod, K. G., Hasegawa, T., Hanson, E. M., Boomer, I., & Kirby, N. (2022). Data report: Cenozoic and Upper Cretaceous bulk carbonate stable carbon and oxygen isotopes from IODP Sites U1513, U1514 and U1516, Expedition 369 in the southeast Indian Ocean. IODP Initial Reports. v. 369. Retrieved from http://iodp.tamu.edu/publications/proceedings

Erbacher, J., & Thurow, J. (1997). Influence of oceanic anoxic events on the evolution of mid-Cretaceous radiolaria in the North Atlantic and western Tethys. *Marine Micropaleontology*, *30*(1–3), 139–158. https://doi.org/10.1016/s0377-8398(96)00023-0

Foster, G. L., Royer, D. L., & Lunt, D. J. (2017). Future climate forcing potentially without precedent in the last 420 million years. *Nature Communications*, *8*, 14845. https://doi.org/10.1038/ncomms14845

Gale, A. S., Bown, P., Caron, M., Crampton, J., Crowhurst, S. J., Kennedy, W. J., et al. (2011). The uppermost Middle and Upper Albian succession at the Col de Palluel, Hautes-Alpes, France: An integrated study (ammonites, inoceramid bivalves, planktonic foraminifera, nannofossils, geochemistry, stable oxygen and carbon isotopes, cyclostratigraphy). *Cretaceous Research*, *32*, 59–130. https://doi.org/10.1016/j.cretres.2010.10.004

Gambacorta, G., Bottini, C., Brumsack, H.-J., Schnetger, B., & Erba, E. (2020). Major and trace element characterization of Oceanic Anoxic Event 1d (OAE 1d): Insight from the Umbria-Marche Basin, central Italy. *Chemical Geology*, *557*. https://doi.org/10.1016/j.chemgeo.2020.119834

Gambacorta, G., Jenkyns, H. C., Russo, F., Tsikos, H., Wilson, P. A., Faucher, G., & Erba, E. (2015). Carbon- and oxygen-isotope records of mid-Cretaceous Tethyan pelagic sequences from the Umbria-Marche and Belluno Basins (Italy). *Newsletters on Stratigraphy*, *48*(3), 299–323. https://doi.org/10.1127/nos/2015/0066

Giorgioni, M., Weissert, H., Bernasconi, S. M., Hochuli, P. A., Keller, C. E., Coccioni, R., et al. (2015). Paleoceanographic changes during the Albian–Cenomanian in the Tethys and North Atlantic and the onset of the Cretaceous chalk. *Global and Planetary Change*, *126*, 46–61. https://doi.org/10.1016/j.gloplacha.2015.01.005

Grasby, S. E., Them, T. R., Chen, Z., Yin, R., & Ardakani, O. H. (2019). Mercury as a proxy for volcanic emissions in the geologic record. *Earth-Science Reviews*, *196*, 102880. https://doi.org/10.1016/j.earscirev.2019.102880

Gröcke, D. R., Ludvigson, G. A., Witzke, B. L., Robinson, S. A., Joeckel, R., Ufnar, D. F., et al. (2006). Recognizing the Albian-Cenomanian (OAE1d) sequence boundary using plant carbon isotopes: Dakota Formation, Western Interior Basin, USA. *Geology.34*, 193–196. https://doi.org/10.1130/G21998.1

Haq, B. U. (2014). Cretaceous eustasy revisited. *Global and Planetary Change*, *113*, 44–58. https://doi.org/10.1016/j.gloplacha.2013.12.007

Huber, B. T., Hobbs, R. W., & Bogus, K. A. (2019). Australia Cretaceous climate and tectonics. In M. R. Hobbs, B. T. Huber, & K. A. Bogus, (Eds.), *Expedition 369 scientists*. *Proceedings of the International Ocean Discovery Program (vol 369, site U1513)*. International Ocean Discovery Program. https://doi.org/10.14379/iodp.proc.369.104.2019

Huber, B. T., MacLeod, K. G., Watkins, D. K., & Coffin, M. F. (2018). The rise and fall of the Cretaceous hot greenhouse climate. *Global and Planetary Change*, *167*, 1–23. https://doi.org/10.1016/j.gloplacha.2018.04.004

Jenkyns, H. C. (2010). Geochemistry of oceanic anoxic events. *Geochemistry, Geophysics, Geosystems*, *11*, Q03004. https://doi.org/10.1029/2009gc002788

Kirkland, C. L., Spaggiari, C. V., Smithies, R. H., Wingate, M. T. D., Belousova, E. A., Greau, Y., et al. (2015). The affinity of Archean of crust on the Yilgarn-Albany-Fraser Orogen boundary: Implications for gold mineralization in the Tropicana zone. *Precambrian Research*, *266*, 260–281. https://doi.org/10.1016/j.precamres.2015.05.023

Koppers, A. A. P., & Coggon, R. (Eds.), (2020). *Exploring earth by scientific ocean drilling: 2050 science framework* (pp. 48–55). https://doi.org/10.6075/J0W66J9H

Lee, E. Y., Wolfgring, E., Tejada, M. L. G., Harry, D. L., Wainman, C. C., Chun, S. S., et al. (2020). Early Cretaceous subsidence of the Naturaliste Plateau defined by a new record of volcaniclastic-rich sequence at IODP Site U1513. *Gondwana Research*, *82*, 1–11. https://doi.org/10.1016/j.gr.2019.12.007

Li, X., Wei, Y., Li, Y., & Zhang, C. (2016). Carbon isotope records of the early Albian oceanic anoxic event (OAE) 1b from eastern Tethys (southern Tibet, China). *Cretaceous Research*, *62*, 109–121. https://doi.org/10.1016/j.cretres.2015.08.015

Lim, D., Kim, J., Xu, Z., Jeong, K., & Jung, H. (2017). New evidence for Kuroshio inflow and deepwater circulation in the Okinawa Trough, East China Sea: Sedimentary mercury variations over the last 20 kyr. *Paleoceanography and Paleoclimatology*, *32*, 571–579. https://doi.org/10.1002/2017pa003116

Lowery, C. M., Bown, P. R., Fraass, A. J., & Hull, P. M. (2020). Ecological response of plankton to environmental change: Thresholds for extinction. *Annual Review of Earth and Planetary Sciences*, *48*, 403–429. https://doi.org/10.1146/annurev-earth-081619-052818

März, C., Schnetger, B., & Brumsack, H.-J. (2013). Nutrient leakage from the North Pacific to the Bering Sea (IODP Site U1341) following the onset of northern hemispheric glaciation? *Paleoceanography*, *28*, 68–78. https://doi.org/10.1002/palo.20011

Morse, J. W., & Berner, R. A. (1995). What determines sedimentary C/S ratios? *Geochimica et Cosmochimica Acta*, *59*(6), 1073–1077. https://doi.org/10.1016/0016-7037(95)00024-t

Mortlock, R. A., & Froelich, P. N. (1989). A simple method for the rapid determination of biogenic opal in pelagic marine sediments. *Deep Sea Research Part I: Oceanographic Research Papers*, *36*(9), 1415–1426. https://doi.org/10.1016/0198-0149(89)90092-7

Müller, P. J., & Schneider, R. (1993). An automated leaching method for the determination of opal in sediments and particulate matter. *Deep Sea Research Part I: Oceanographic Research Papers*, *40*(3), 425–444. https://doi.org/10.1016/0967-0637(93)90140-x

Munksgaard, N. C., Lim, K., & Parry, D. L. (2003). Rare Earth elements as provenance indicators in North Australian estuarine and coastal marine sediments. *Estuarine, Coastal and Shelf Science*, *57*(3), 399–409. https://doi.org/10.1016/s0272-7714(02)00368-2

Navarro-Ramirez, J. P., Bodin, S., Heimhofer, U., & Immenhauser, A. (2015). Record of Albian to early Cenomanian environmental perturbation in the eastern sub-equatorial Pacific. *Palaeogeography, Palaeoclimatology, Palaeoecology*, *423*, 122–137. https://doi.org/10.1016/j.palaeo.2015.01.025

Neal, C. R., Mahoney, J. J., & Chazey, W. J. (2002). Mantle Sources and the highly variable role of continental lithosphere in Basalt Petrogenesis of the Kerguelen Plateau and Broken Ridge LIP: Results from ODP Leg 183. *Journal of Petrology*, *43*(7), 1177–1205. https://doi.org/10.1093/petrology/43.7.1177

Nesbitt, H. W., & Young, G. M. (1982). Early Proterozoic climates and plate motions inferred from major element chemistry of lutites. *Nature*, *299*(5885), 715–717. https://doi.org/10.1038/299715a0

O'Brien, C. L., Robinson, S. A., Pancost, R. D., Sinninghe Damsté, J. S., Schouten, S., Lunt, D. J., et al. (2017). Cretaceous sea-surface temperature evolution: Constraints from TEX86 and planktonic foraminiferal oxygen isotopes. *Earth-Science Reviews*, *172*, 224–247. https://doi.org/10.1016/j.earscirev.2017.07.012

Olierook, H. K., Barham, M., Fitzsimons, I. C., Timms, N. E., Jiang, Q., Evans, N. J., & McDonald, B. J. (2019). Tectonic controls on sediment provenance evolution in rift basins: Detrital zircon U–Pb and Hf isotope analysis from the Perth Basin, Western Australia. *Gondwana Research*, *66*, 126–142. https://doi.org/10.1016/j.gr.2018.11.002

Pavlishina, P. (2017). Palynostratigraphy and palaeoenvironments around the Albian-Cenomanian boundary interval (OAE 1d), North Bulgaria. *Science China Earth Sciences*, *60*, 71–79. https://doi.org/10.1007/s11430-016-0067-2

Petrizzo, M. R., Huber, B. T., Wilson, P. A., & MacLeod, K. G. (2008). Late Albian paleoceanography of the western subtropical North Atlantic. *Paleoceanography*, *23*, PA1213. https://doi.org/10.1029/2007PA001517

Pyle, D. G., Christie, D. M., Mahoney, J. J., & Duncan, R. A. (1995). Geochemistry and geochronology of ancient southeast Indian and southwest Pacific seafloor. *Journal of Geophysical Research*, *100*, 22261–22282. https://doi.org/10.1029/95jb01424

Qiu, Y., McNaughton, N., Groves, D., & Dunphy, J. (1999). First record of 1.2 Ga quartz dioritic magmatism in the Archaean Yilgarn Craton, Western Australia, and its significance. *Australian Journal of Earth Sciences*, *46*, 421–428. https://doi.org/10.1046/j.1440-0952.1999.00715.x

Rea, D. K., & Janecek, T. R. (1981). Mass-accumulation rates of the non-authigenic inorganic crystalline (eolian) component of deep-sea sediments form the western mid-Pacific mountains, Deep Sea Drilling Project Site 463. In J. Thiede, T. L. Valuer, C. G. Adelseck, A. Boersma, P. Čepek, W. E. Dean, et al. (Eds.), (Vol. 62, pp. 653–659). U.S. Government Printing Office. https://doi.org/10.2973/dsdp.proc.62.125.1981. *Initial Reports of the Deep Sea Drilling Project*

Richey, J. D., Upchurch, G. R., Montanez, I. P., Lomax, B. H., Suarez, M. B., Crout, N. M., et al. (2018). Changes in $CO_2$ during ocean anoxic event 1d indicate similarities to other carbon cycle perturbations. *Earth and Planetary Science Letters*, *491*, 172–182. https://doi.org/10.1016/j.epsl.2018.03.035

Rodríguez-Cuicas, M.-E., Montero-Serrano, J.-C., & Garbán, G. (2019). Paleoenvironmental changes during the late Albian oceanic anoxic event 1d: An example from the Capacho Formation, southwestern Venezuela. *Palaeogeography, Palaeoclimatology, Palaeoecology*, *521*, 10–29. https://doi.org/10.1016/j.palaeo.2019.02.010

Rodríguez-Cuicas, M.-E., Montero-Serrano, J.-C., & Garbán, G. (2020). Geochemical and mineralogical records of late Albian oceanic anoxic event 1d (OAE-1d) in the La Grita Member (southwestern Venezuela): Implications for weathering and provenance. *Journal of South American Earth Sciences*, *97*, 102408. https://doi.org/10.1016/j.jsames.2019.102408

Scaife, J. D., Ruhl, M., Dickson, A. J., Mather, T. A., Jenkyns, H. C., Percival, L. M. E., et al. (2017). Sedimentary mercury enrichments as a marker for submarine large igneous province volcanism? Evidence from the Mid-Cenomanian event and Oceanic Anoxic Event 2 (Late Cretaceous). *Geochemistry, Geophysics, Geosystems*, *18*, 4253–4275. https://doi.org/10.1002/2017gc007153

Schlanger, S., & Jenkyns, H. C. (1976). Cretaceous oceanic anoxic events: Causes and consequences. *Geologie en Mjinbouw*, *55*(3–4), 179–184. Retrieved from https://www.researchgate.net/publication/27710997_Cretaceous_Oceanic_Anoxic_Events_Causes_and_consequences

Scotese, C. (2016). *PALEOMAP PaleoAtlas for GPlates and the PaleoData plotter Program, PALEOMAP Project. 50th Annual GSA North-Central Section Meeting*. Retrieved from https://www.earthbyte.org/category/resources/data-models/paleogeography/

Scott, R. W., Formolo, M., Rush, N., Owens, J. D., & Oboh-Ikuenobe, F. (2013). Upper Albian OAE 1d event in the Chihuahua Trough, New Mexico, USA. *Cretaceous Research*, *46*, 136–150. https://doi.org/10.1016/j.cretres.2013.08.011

Smithies, R., Spaggiari, C., & Kirkland, C. (2015). *Building the crust of the Albany-Fraser Orogen; constraints from granite geochemistry*. Geological Survey of Western Australia

Storey, M. (1992). Lower Cretaceous volcanic rocks on continental margins and their relationship to the Kerguelen plateau. *Proceedings of the Ocean Drilling Program, Scientific Results*, *120*, 33–53. https://doi.org/10.2973/odp.proc.sr.120.118.1992

Stuut, J., Temmesfeld, F., & Deckker, P. D. (2014). A 550 ka record of aeolian activity near North west Cape, Australia: Inferences from grain-size distributions and bulk chemistry of SE Indian Ocean deep-sea sediments. *Quaternary Science Reviews*, *83*, 83–94. https://doi.org/10.1016/j.quascirev.2013.11.003

Suan, G., Schollhorn, I., Schlogl, J., Segit, T., Mattioli, E., Lecuyer, C., & Fourel, F. (2018). Euxinic conditions and high sulfur burial near the European shelf margin (Pieniny Klippen Belt, Slovakia) during the Toarcian oceanic anoxic event. *Global and Planetary Change*, *170*, 246–259. https://doi.org/10.1016/j.gloplacha.2018.09.003

Taylor, S. R., & Mclennan, S. M. (1985). The continental crust: Its composition and evolution. *The Journal of Ceology*, *94*(4), 57–72.

Tierney, J. E., Poulsen, C. J., Montanez, I., Bhattacharya, T., Feng, R., Ford, H. L., et al. (2020). Past climates inform our future. *Science*, *370*, eaay3701. https://doi.org/10.1126/science.aay3701

Turgeon, S., & Brumsack, H. J. (2006). Anoxic vs dysoxic events reflected in sediment geochemistry during the Cenomanian–Turonian Boundary Event (Cretaceous) in the Umbria–Marche Basin of central Italy. *Chemical Geology*, *234*(3–4), 321–339. https://doi.org/10.1016/j.chemgeo.2006.05.008

Van Helmond, N. A. G. M., Sluijs, A., Sinninghe Damsté, J. S., Reichart, G.-J., Voigt, S., Erbacher, J., et al. (2015). Freshwater discharge controlled deposition of Cenomanian–Turonian black shales on the NW European epicontinental shelf (Wunstorf, northern Germany). *Climate of the Past*, *11*, 495–508. https://doi.org/10.5194/cp-11-495-2015

Wan, S., Clift, P. D., Zhao, D., Hovius, N., Munhoven, G., France-Lanord, C., et al. (2017). Enhanced silicate weathering of tropical shelf sediments exposed during glacial lowstands: A sink for atmospheric $CO_2$. *Geochimica et Cosmochimica Acta*, *200*, 123–144. https://doi.org/10.1016/j.gca.2016.12.010

Wehausen, R., Tian, J., Brumsack, H.-J., Cheng, X., & Wang, P. (2003). Geochemistry of Pliocence sediments from ODP site 1143 (Southern South China Sea). *Proceedings of the Ocean Drilling Program, Science Results*, *184*, 1–25. Retrieved from http://www-odp.tamu.edu/publications/184_SR/VOLUME/CHAPTERS/201.PDF

Wilde, S., & Nelson, D. (2001). *Geology of the western Yilgarn Craton and Leeuwin Complex, Western Australia- a field guide*. Geological Survey of Western Australia

Wilson, P. A., & Norris, R. D. J. (2001). Warm tropical ocean surface and global anoxia during the mid-Cretaceous period. *Nature*, *412*, 425–429. https://doi.org/10.1038/35086553

Xu, Z., Li, T., Clift, P. D., Wan, S., Lim, D., & Lim, D. (2018). Bathyal records of enhanced silicate erosion and weathering on the exposed Luzon shelf during glacial lowstands and their significance for atmospheric $CO_2$ sink. *Chemical Geology*, *476*, 302–315. https://doi.org/10.1016/j.chemgeo.2017.11.027

Xu, Z., Wan, S., Colin, C., Li, T., Clift, P. D., Chang, F., et al. (2020). Enhanced terrigenous organic matter input and productivity on the western margin of the Western Pacific Warm Pool during the Quaternary sea-level lowstands: Forcing mechanisms and implications for the global carbon cycle. *Quaternary Science Reviews*, *232*, 106211. https://doi.org/10.1016/j.quascirev.2020.106211

Yao, H., Chen, X., Melinte-Dobrinescu, M. C., Wu, H., Liang, H., & Weissert, H. (2018). Biostratigraphy, carbon isotopes and cyclostratigraphy of the Albian-Cenomanian transition and Oceanic Anoxic Event 1d in southern Tibet. *Palaeogeography, Palaeoclimatology, Palaeoecology*, *499*, 45–55. https://doi.org/10.1016/j.palaeo.2018.03.005

Yao, H., Chen, X., Yin, R., Grasby, S. E., Weissert, H., Gu, X., et al. (2021). Mercury evidence of intense volcanism preceded Oceanic Anoxic Event 1d. *Geophysical Research Letters*, *48*(5), e2020GL091508. https://doi.org/10.1029/2020gl091508

Zhang, X., Li, S., Wang, X., Zhao, X., & Yin, T. (2021). Expression of the early Aptian Oceanic Anoxic Event (OAE) 1a in lacustrine depositional systems of East China. *Global and Planetary Change*, *196*, 103370. https://doi.org/10.1016/j.gloplacha.2020.103370